AIP | Applied Physics Letters

Epitaxial Pb(Mg1/3Nb2/3)O3-PbTiO3 (67/33) thin films with large tunable self-bias field controlled by a PbZr1xTixO3 interfacial layer

M. Boota, E. P. Houwman, M. Dekkers, M. Nguyen, and G. Rijnders

Citation: Applied Physics Letters **104**, 182909 (2014); doi: 10.1063/1.4874978
View online: http://dx.doi.org/10.1063/1.4874978
View Table of Contents: http://scitation.aip.org/content/aip/journal/apl/104/18?ver=pdfcov
Published by the AIP Publishing

Epitaxial $Pb(Mg_{1/3}Nb_{2/3})O_3$-$PbTiO_3$ (67/33) thin films with large tunable self-bias field controlled by a $PbZr_{1-x}Ti_xO_3$ interfacial layer

M. Boota,[1,2] E. P. Houwman,[1] M. Dekkers,[3] M. Nguyen,[1,3] and G. Rijnders[1,a)]
[1]*MESA+ Institute for Nanotechnology, University of Twente, P.O. Box 217, 7500AE Enschede, The Netherlands*
[2]*Engineering Department, University of Rome "ROMA TRE," Via Della Vasca Navale 79, 00146 Rome, Italy*
[3]*SolMates BV, Drienerlolaan 5, Building 6, 7522NB Enschede, The Netherlands*

(Received 27 February 2014; accepted 31 March 2014; published online 8 May 2014)

Epitaxial $Pb(Mg_{1/3}Nb_{2/3})O_3$-$PbTiO_3$ 200 nm thick, (001) oriented, perovskite phase-pure films were grown on a range of $PbZr_{1-x}Ti_xO_3$ buffer layers ($x = 0.2$–0.8) and sandwiched between $SrRuO_3$ electrodes on (001) $SrTiO_3$ substrates to form a ferroelectric capacitor structure. Devices without a buffer layer or with a buffer layer of highly tetragonal $PbZr_{1-x}Ti_xO_3$ show very large self-bias fields up to 1.0×10^7 V/m. These self-bias fields correlate with strain gradient layers near the bottom electrode observed in these devices only. The large self-bias was explained quantitatively in terms of the flexoelectric effect. © *2014 AIP Publishing LLC*. [http://dx.doi.org/10.1063/1.4874978]

Ferroelectric oxides, most notably $PbZr_{1-x}Ti_xO_3$ (PZT), are very useful for micro electromechanical systems (MEMS) for the purpose of sensing and actuation.[1,2] An alternative to PZT is a relaxor ferroelectric like $Pb(Mg_{1/3}Nb_{2/3})O_3$-$PbTiO_3$ (PMN-PT), which is a solid solution between a relaxor (PMN) and a ferroelectric (PT) material. Recent developments in relaxor ferroelectrics yielding giant piezoelectric response have propelled them to the forefront for sensor and actuator research and development.[3–5] Bulk PMN-PT can demonstrate an enormous strain level (≈1.7%), and its piezoelectric coefficients can be five to ten times larger than bulk PZT ceramics. The large electromechanical coupling coefficient ($k_{33} \approx 0.9$) of PMN-PT promises exciting applications.[3] At low temperatures, PMN-PT is rhombohedral up to some specific PT concentration. Above this concentration, it undergoes a morphotropic phase transition and becomes tetragonal.[6] In the bulk PMN-PT ceramic solid solution system, the morphotropic phase boundary occurs at 33% PT.[7] The giant piezoelectric response in PMN-PT ceramics has been observed near this morphotropic phase boundary, in particular in single crystalline material with (001) orientation rather than in polycrystalline samples.[3,5]

For many applications, one requires materials in thin film form. It is well known that the properties of the PMN-PT thin films depend upon factors such as chemical composition, stoichiometry, phase purity, defect density, orientation, and mechanical boundary conditions. One of the major difficulties in fabricating PMN-PT thin films is the purity of the perovskite phase, and the most prominent second phase that typically appears during synthesis is the pyrochlore phase. This lead deficient, non-piezoelectric phase ($Pb_2Nb_2O_7$) forms due to ineffective incorporation of volatile constituents (for instance, PbO) into the film,[8] and its presence degrades the piezoelectric properties. The multistep columbite process was developed for the synthesis of the pure bulk perovskite phase PMN-PT ceramic that bypasses the pyrochlore phase formation by facilitating the reaction between magnesium, niobium, and lead oxides.[8] However, this method is not suitable for thin film synthesis. Bu *et al.* and Baek *et al.*[4,5] demonstrated the perovskite phase stabilization in PMN-PT films deposited on miscut $SrTiO_3$ (STO) and Si substrates, respectively. There, the high density of steps on the (miscut Si) surface helps to maintain film stoichiometry due to the effective incorporation of volatile constituents (PbO).

In the present work, we achieve a (001) oriented, pure perovskite phase of epitaxial PMN-PT (67/33) thin films on (001) oriented STO low miscut substrates by carefully optimizing the film growth conditions. Secondly, we use a PZT buffer layer of varying composition that introduces a large build-in self-bias field for tetragonal compositions. This self-bias field is remarkably stable on prolonged cycling and can be tuned by the PZT composition. Such a tunable self-bias is of great importance for devices like energy harvesters, which are operated at zero bias. By tuning the self-bias, one can optimize the operation point and potentially the device performance.

Capacitor stacks of a 100 nm $SrRuO_3$ (SRO) base electrode, 25 nm thick PZT buffer layer, 200 nm PMN-PT, and a 100 nm thick SRO top electrode were grown on TiO_2 terminated (001) oriented STO substrates[9] (samples S1–S6). Further, one sample with a 1% Nb-doped PZT (52:48) buffer layer was prepared (sample S4N) and one without buffer layer (S0). We have used a growth process of the PMN-PT layer that was optimized for phase purity, film smoothness, and maximum piezoelectric coefficient d_{33}. There is a relatively narrow process window around the following process parameter values: All layers are subsequently deposited by pulsed laser deposition using a KrF Excimer laser (248 nm) without breaking the vacuum. The PMN-PT films were deposited at a substrate temperature of 600 °C, at a pure oxygen pressure of 0.28 millibar, a target-substrate distance of 6 cm, and at a laser fluence of 2.25 J/cm^2 at 4 Hz repetition rate. The deposition conditions of the PZT buffer layers are similar except for the oxygen pressure (0.10 millibar). The deposition conditions of the SRO electrodes are reported elsewhere.[10] The layer stack is cooled down from deposition temperature to room temperature in a 1 bar pure oxygen atmosphere. The

a)E-mail: a.j.h.m.rijnders@utwente.nl

capacitor structures are defined by photolithography and Ar ion beam etching.

X-ray diffraction (XRD) θ-2θ, azimuthal φ-scans, rocking curves, and reciprocal space mapping were performed to determine the crystallographic structure of the stack. Part of the θ-2θ spectra of the film stacks with and without PZT interfacial layer is shown in Fig. 1. The reflections from the substrate, electrodes, PZT interfacial layer, and PMN-PT peaks are indicated. In the full spectrum (not shown), the PMN-PT reflections can all be attributed to (001) growth orientation. No additional peaks representing secondary phases (pyrochlore phase) or orientations are detected. φ-scans show in-plane epitaxy with a cube on cube relation with the substrate. Rocking curves of the PMN-PT reflections have a full width at half maximum of 0.05°–0.21° for the films with PZT buffer layer and 0.52° for the PMN-PT film deposited directly on the SRO bottom electrode. The narrowness of these peaks demonstrates the high degree of oriented growth and good crystallinity of these films.

From Fig. 1, it is seen that the PMN-PT reflections in most cases are slightly shifted from the angle expected for rhombohedral, unstrained PMN-PT. The broad shoulder at lower angles causing the asymmetric PMN-PT reflection for samples with PZT($x \geq 0.6$) and for sample S0, without PZT, indicates compressive strain relaxation from the in-plane lattice constant of the underlying (PZT or SRO) layer to that of the bulk value of PMN-PT. The XRD data of the sample S4N (not shown) are practically equal to that of S4, thus the doping does not influence the lattice parameters and the strain state. For buffer layers PZT ($x < 0.6$), there is a small in-plane tensile strain in the PMN-PT layer and thus a marginally decreased out-of-plane lattice parameter. In the θ-2θ for films with PZT ($x < 0.5$), a single PZT reflection (intensity $I_1(x)$) is observed, whereas for the tetragonal compositions a second, weaker peak ($I_2(x)$) appears with a larger out-of-plane lattice constant. For the tetragonal compositions, there is no signature of structural domains with the long axis in plane (*a* domains), which would show up near the angles indicated by $a_{tetr.PZT,\ unstrained}$. The main out-of-plane reflections for $x = 0.7$ and 0.8 correspond well with an unstrained long-axis value of the unit cell ($c_{tetr.PZT,unstrained}$). The second lower intensity peak corresponds to strong in-plane compression with an in-plane lattice parameter of about 3.95 Å, approaching that of the STO substrate (3.905 Å). (If the PZT were fully strained to the substrate, the out-of-plane reflection would appear at the positions denoted by $c_{PZT\ strained\ to\ STO}$.) The broad plateau in between the peaks ($x = 0.7$ and 0.8) and the wide shoulder (for $x = 0.6$) at the low angle side of the main PZT reflection of the tetragonal composition films is attributed to a gradual strain relaxation from the highly strained layer to the bulk of the film. For $x = 0.6$ and 0.5, the PZT is slightly tensile strained and the films with rhombohedral PZT compositions are slightly compressively strained. The measured *c*/*a* ratios of the PMN-PT and PZT-films are depicted in Fig. 2(a), together with the values for bulk PZT.[11] In Fig. 2(b), the unit cell volumes (V_{uc}) are given, showing constant V_{uc}(PMN-PT) and bulk V_{uc}(PZTx) corresponding to the I_1 reflections. The data points corresponding to the reflections I_2 on the other hand correspond to an extremely large compressive strain (large (*c*/*a*) and slightly enhanced V_{uc}.

The XRD analysis indicates that the PZT layers with rhombohedral compositions and the main part of the tetragonal PZT films are slightly strained. The tetragonal films with large bulk *c*/*a* ratio show a relaxing strain gradient with maximum strain at the base electrode/PZT interface, relaxing into the film. Strain relaxation occurs by the incorporation of lattice defect, which are generally accompanied by defect charges. Further, the high strain and an increased defect density increase the PZT unit cell volume.

The polarization hysteresis loops were measured from which the self-bias field $E_{sb} = (E_c^+ - E_c^-)/2$ and the coercive field $E_{c,av} = (E_c^+ - E_c^-)/2$ were obtained. In Fig. 3(a), the self-bias field and the coercive field are shown as function of the PZT-composition of the buffer layer. The devices with large E_c correspond to those with a large strain relaxation layer at the base-electrode/ferroelectric interface, both in the devices with (S1 and S2) and without PZT-buffer layer (S0). The devices with predominantly constant (small) strain in the PZT and PMN-PT layers (S3 to S6) have negligible self-bias. The coercive field shows a similar trend. The Nb-doped device S4N has an increased negative self-bias field as compared to the undoped comparison sample S4. The coercive field of S4N is reduced with respect to that of S4. In Figs. 3(b) and 3(c) E_c and E_{sb} are shown as a function of the number of aging cycles (cycling through the complete PE-loop up to +/−500 kV/cm) for the devices S0, S1, S2, and S5. The devices S0, S3-6, and S4N are very stable up to the maximum number of cycles, 10^8, implying that the charge density profile in the device is very stable upon cycling. For S1 as well as S2, the self-bias and coercive field both decrease monotonically upon cycling and stabilize after about 10^7–10^8 cycles, which indicates that a new, stable (charge) configuration has been established. The large coercive field values of the devices S1 and S2 appear to be correlated with the large E_{sb}. For $E_c < 2.5$ MV/m, another pinning

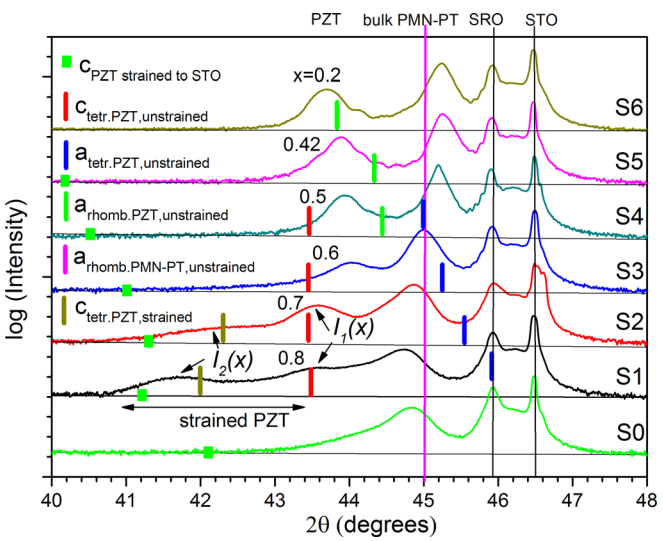

FIG. 1. XRD spectra of 200 nm PMN-PT ferroelectric capacitors on STO substrates with 100 nm SRO electrodes without (sample S0) and with (S1-S6) 25 nm PZT buffer layers. The bars indicate the positions of reflection peaks of unstrained PZT and PMN-PT films. The square denotes the position of PZT and PMN-PT strained fully to the substrate.

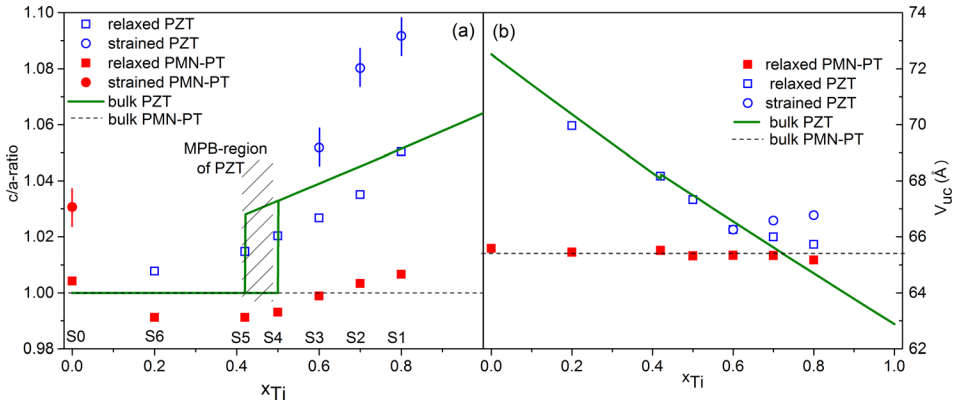

FIG. 2. (a) Measured c/a ratio of the out-of-plane and in-plane lattice parameters (c/a ratio) of the largely relaxed bulk, respectively, strained fractions of the PZT and PMN-PT films in the PZT/PMN-PT ferroelectric capacitors. The curves for PZT are from Ref. 11. The hatched region denotes the region around the Morphotropic Phase Boundary. (b) Measured unit cell volume of the largely relaxed bulk, respectively, strained fractions of the PZT and PMN-PT films.

mechanism is dominant, that is apparently not linked to the charge density.

In spite of many theoretical and experimental works on possible causes of field self-bias in ferroelectric capacitors, the physical mechanism behind the built-in fields is often hard to identify, since many extrinsic and intrinsic factors may play a role.[12] In the devices S0, S1, and S2, we identified compressively strained layers next to the base electrode. In such a layer, the strain is relaxed by dislocations, which can be accompanied by charged defects. This charged layer might be the (extrinsic) mechanism behind the field bias. On the other hand, the strain gradient can also give rise to an internal field. This is then considered an internal cause.

Assuming that the self-bias is due to a homogeneous charge distribution $\rho(x)$ due to dislocations in the strain relaxation layer with thickness a_ρ, we calculated the field outside this layer as

$$\vec{E}_\rho = \frac{\rho a_\rho}{\varepsilon_0 \varepsilon_b} \frac{a_\rho}{2L} \vec{e}_x \quad x > a_\rho, \tag{1}$$

where ε_b is the dielectric constant of the background dielectric (assumed to be constant over the total stack thickness L) which is of the order of 10.[12] The thickness a_ρ is a fraction of the PZT layer thickness and is estimated from the integrated XRD intensity ratio to be 5 and 10 nm respectively for S1 and S2 and 16 nm for S0. Since a_ρ/L is small, the observed self-bias field is then largely due to the constant field for $x > a_\rho$. The space charge density is estimated from the measured self-bias field to be of the order of $\rho = 1.6 \times 10^7$ C/m^3 or 6.4×10^{-3} |e|/unit cell for sample S1 with the largest bias field, $E_{sb} = 101$ kV/cm. This corresponds to a positive charge of one |e| in each cube of $5.4 \times 5.4 \times 5.4$ unit cells. This charged defect density is consistent with defects concentrated in the grain boundaries and defect planes, which create the necessary stress relaxation. Upon continuous cycling, the self-bias and coercive field decreases. This can be interpreted as being due to compensation of the positive charges in the strained layer by electrons injected from the electrode in an irreversible process. The coercive field decreases due to reduced pinning of the domain walls at the reduced density of charged defects. In this picture, the very small self-bias fields for S3-6 ($|E_{sb}| < 10^6$ V/m) are ascribed to a very thin, lightly charged layer, or "dead" (passive) dielectric layer adjacent to the electrodes and/or dielectric grain boundaries.[12]

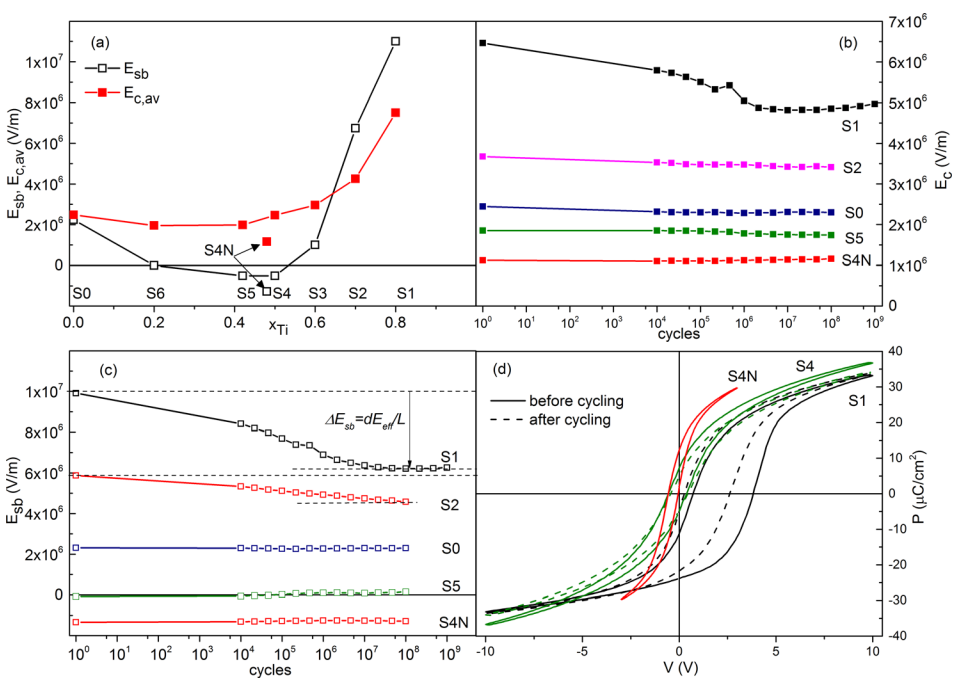

FIG. 3. (a) Measured self-bias field E_{sb} and coercive field E_c (before aging) of PZT/PMN-PT ferro-electric capacitors. The lines are guides to the eye. (b) Coercive field E_c and (c) Self-bias field E_{sb} as function of number of cycling (up to $+/-5 \times 10^7$ V/m). (d) Polarization loops before and after cycling.

The observed strain gradient in the devices with large self-bias suggests a second possible cause, the flexoelectric effect.[12–14] Here, we follow the model of Ref. 12. Due to the strain gradient in the stress relaxation layer at the bottom electrode, a large effective electrical field E_{eff} is created in this layer (with thickness d, approximately equal to a_ρ) through the flexoelectric effect

$$E_{\text{eff}} = E_3 = \phi_{11}\frac{\partial S_3}{\partial x_3} + 2\phi_{12}\frac{\partial S_1}{\partial x_3}. \quad (2)$$

Here, ϕ_{ij} are the strain gradient electric field coupling coefficients. The out-of-plane gradient term can be estimated as $\partial S_3/\partial x_3 \approx \Delta S_3/d = (c(d)) - c(0))/a_c d$, where $c(0)$ is the (measured) c–axis length of the strained layer with thickness d and $c(d)$ that of the unstrained PZT and the in-plane gradient term as $\partial S_1/\partial x_3 = \Delta S_1/d = (a(d) - a(0))/a_c d$, where a is the measured in-plane lattice parameter. The values of the flexoelectric tensor components have been estimated as $|\phi_{ij}/a_c| = E_{at}$. E_{at} is a typical atomic electric field of about 100MV/cm for perovskites and a_c is the pseudocubic lattice parameter. Further, it is reasonable to assume that ϕ_{12} has a sign opposite to that of ϕ_{11}. The resulting estimate of the absolute value of the effective field in the strained layer is $|E_{\text{eff}}| = |E_{at}(\Delta S_3 - 2\Delta S_1)(a_c/d)| = 4.6 \times 10^7$ V/m for S1. The effective field can be so large that the thin layer becomes non-switchable for all applied external field values with a fixed polarization P_M. Further, at the interface of the non-switchable layer and the switchable layer, a free charge layer with charge density σ may be present. The self-bias voltage V_{sb} (or (apparent) self-bias field $E_{sb} = V_{sb}/L$) is given by[15]

$$V_{sb} = \frac{d}{\varepsilon_0 \varepsilon_{\text{f,str}}}(P_M + \sigma) + dE_{\text{eff}}, \quad (3)$$

where $\varepsilon_{\text{f,str}}$ is the relative dielectric constant of the strained layer. We have observed that over time V_{sb} changes with cycling and reaches a new, lower, stable value. Following the suggestion of Ref. 12, we assume that in the initial state the free (interface) charge density is (negligible) small, hence a large initial self-bias voltage, $V_{sb}^{ini} = dP_M/\varepsilon_0\varepsilon_{f,str} + dE_{\text{eff}}$, is present. After long cycling, free charge builds up and compensates the field in the strained layer, reaching a value $\sigma = -\varepsilon_0\varepsilon_{f,str}E_{\text{eff}}$, so that the final self-bias voltage is $V_{sb}^{fin} = dP_M/\varepsilon_0\varepsilon_{f,str}$. From the measured self-bias voltages and strained layer thickness, we estimate $E_{\text{eff}} = 1.7 \times 10^8$ V/m for S1. This is only a factor of 3 larger than the value estimated above from the flexoelectric effect. Assuming the value of P_M to be equal to the spontaneous polarization $P_s = 0.70\,\text{C/m}^2$ of bulk material,[16] one obtains $\varepsilon_{f,str} = 274$ and $\sigma = -0.40\,\text{C/m}^2$. This suggests that the permittivity of the strain-gradient layer is significantly enhanced over that of the bulk value ($\varepsilon_{f,bulk} = 86$ for $x = 0.8$).[16] This may be ascribed to the fact that the layer is not only subjected to a strain-gradient but also to a very large strain, considering that the c/a ratio reaches a value of approximately 1.09 in this layer. The large self-bias voltage of S2 and its cycling dependence can be explained in the same way. S0 does not show any cycling dependence of E_{sb}, suggesting that the displacement of free charges does not take place. The self-bias voltage of S0 is low compared to the initial V_{sb} values in S1 and S2. The lowest value that can be obtained is when E_{eff} is fully compensated by trapped free charge from the very first fatigue cycle onwards, thus $V_{sb} = dP_M/\varepsilon_0\varepsilon_{f,str}$. In this case, the polarization is directed approximately in the body diagonal of the rhombohedrally distorted pseudocubic lattice of PMN-PT, hence $P_M \approx P_S/\sqrt{3} = 0.32\,\text{C/m}^2$. With this value one obtains $\varepsilon_{f,str} = 1240$, a factor of 2 larger than the literature value 680 for poled PMN-PT.[17] From this argument, one has to conclude that already during cooldown after fabrication of the S0 device free charge is trapped in the PMN-PT that compensates the effective field. The samples S3-6 do not show any significant self-bias nor any significant strain gradient in the PZT and the PMN-PT layer. This is taken as a strong indication that the strain gradient is the dominating mechanism behind the large self-biases in the devices S0-2.

The observation that the very thin tetragonal PZT layers (S1-2) grow in a single c-domain phase with the long axis out-of -plane is in accordance with the model of Perstev *et al.*[18] for strained, single domain PZT thin films. In this model, there is a transition to the (rhombohedral) r-phase for PZT($x \approx 0.6$) on STO. We observe a transition at approximately this value from the highly strained initial growth layer to what can be interpreted as a slightly tetragonally distorted rhombohedral phase, in accordance with this model. Further, it appears that in the samples S1-2 the high initial strain relaxes largely within the first 5–10 nm, whereas in S3-6 it is practically immediately relaxed, which is indicative for a high density of misfit dislocations ρ and therefore short strain relaxation layer thickness. The 1% Nb–doped PZT($x = 0.5$) sample S4N shows a negative self-bias field that slightly decreases from -1.34 MV/m to -1.28 MV/m after 10^8 cycles. The XRD data do not give any indications of a strain gradient layer therefore we ascribe the self-bias to the charged Nb–doped PZT-layer. Using Eq. (1) in the small thickness approximation of the charged layer, one obtains a charge density $\rho = -8.5 \times 10^4$ C/m^3 or 3.4×10^{-5} electron/unit cell. This implies that the 1% Nb doping, causing an electron doping of 1 electron per 100 unit cells, is largely cancelled. All the doped electrons are apparently strongly trapped to compensate the positive charges of the Nb-ions and even some extra electron charge is permanently trapped in the Nb–doped PZT layer that creates the small negative charge density in the Nb-doped layer, causing the self-bias.

In conclusion, we have grown ferroelectric capacitors consisting of a 25 nm PZT buffer layer of varying composition and a 200 nm PMN-PT (67:33) layer on STO substrates. XRD analysis shows that all layers are grown with (001) orientation. The PMN-PT layers are perovskite phase pure and do not show any signatures of the pyrochloric phase. The PZT buffer layers with tetragonal composition are initially compressively strained to the substrate and relax fully over the layer thickness. The PZT layers with nearly cubic bulk lattice structure are only slightly and homogeneously strained. The samples with strain gradients near the bottom electrode show large and fairly stable self-bias voltages. The large self-bias samples also show strongly increased coercive fields. The large self-bias was discussed in two ways. First, in the strain

gradient regions the enhanced defect density can be associated with trapped charges. However, in this model the charge density and its sign are free parameters. Second, the strain gradient layers can create a self-bias field through the flexoelectric effect. The observed self-bias voltages are consistent with the measured strain gradients and layer thicknesses. The self-bias voltage can be tuned in a fairly wide range by the composition of the buffer layer. This is of significance for devices like energy scavengers and low energy consumption sensors that preferably operate at zero bias voltage.

This work was supported by the Engineering Doctorate School of Roma TRE University and by NanoNextNL, a micro and nanotechnology consortium of the Government of the Netherlands and 130 partners.

[1]M. D. Nguyen, H. N. Vu, D. H. A. Blank, and G. Rijnders, Adv. Nat. Sci.: Nanosci. Nanotechnol. **2**, 015005 (2011).
[2]D. Isarakorn, A. Sambri, P. Janphuang, D. Briand, S. Gariglio, J.-M. Triscone, F. Guy, J. W. Reiner, C. H. Ahn, and N. F. de Rooij, J. Micromech. Microeng. **20**, 055008 (2010).
[3]S. E. Park and T. R. Shrout, J. Appl. Phys. **82**, 1804 (1997).
[4]S. D. Bu, M. K. Lee, and C. B. Eom, Appl. Phys. Lett. **79**, 3482 (2001).
[5]S. H. Baek, J. Park, D. M. Kim, V. A. Aksyuk, R. R. Das, S. D. Bu, D. A. Felker, J. Lettieri, V. Vaithyanathan, S. S. N. Bharadwaja, N. Bassiri-Gharb, Y. B. Chen, H. P. Sun, C. M. Folkman, H. W. Jang, D. J. Kreft, S. K. Streiffer, R. Ramesh, X. Q. Pan, S. Trolier-McKinstry, D. G. Schlom, M. S. Rzchowski, R. H. Blick, and C. B. Eom, Science **334**, 958 (2011).
[6]Z. Kutnjak, J. Petzelt, and R. Blink, Nature **441**, 956 (2006).
[7]S. E. Park and T. R. Shrout, IEEE Trans. Ultrason. Ferroelectr. Freq. Control **44**, 1140 (1997).
[8]S. L. Swartz and T. R. Shrout, Mater. Res. Bull. **17**, 1245 (1982).
[9]G. Koster, B. L. Kropman, G. J. H. M. Rijnders, D. H. A. Blank, and H. Rogalla, Appl. Phys. Lett. **73**, 2920 (1998).
[10]M. D. Nguyen, H. Nazeer, K. Karakaya, S. V. Pham, R. Steenwelle, M. Dekkers, L. Abelmann, D. H. A. Blank, and G. Rijnders, J. Micromech. Microeng. **20**, 085022 (2010).
[11]G. A. Rossetti, A. G. Khachaturyan, G. Akcay, and Y. Ni, J. Appl. Phys. **103**, 114113 (2008).
[12]A. K. Tagantsev and G. Gerra, J. Appl. Phys. **100**, 051607 (2006).
[13]K. Abe, N. Yanase, T. Yasumoto, and T. Kawakubo, J. Appl. Phys. **91**, 323 (2002).
[14]W. Ma, Phys. Status Solidi B **245**, 761 (2008).
[15]In contrast with Ref. 12 in our configuration, the bottom electrode is grounded; therefore, the signs of all voltages are inverted. In Ref. 13 an interface charge is assumed to be present. Here, it is more likely that the charge is distributed over the strained layer, which is expected to have a similar effect on the self-bias.
[16]M. J. Haun, E. Furman, S. J. Jang, and L. E. Cross, Ferroelectrics **99**, 63 (1989).
[17]H. Cao, V. H. Schmidt, R. Zhang, W. Cao, and H. Luo, J. Appl. Phys. **96**, 549 (2004).
[18]N. A. Perstev, V. G. Kukhar, H. Kohlstedt, and R. Waser, Phys. Rev. B **67**, 054107 (2003).